Stressing the differences in alizarin and purpurin dyes through UV-visible light absorption and ^{1}H-NMR spectroscopies†

Roger-Charles Tissier,[a] Baptiste Rigaud,[b] Pierre Thureau,[a] Maguy Jaber,[b] and Nicolas Ferré*[a]

Three anthraquinone-based chromophores (9,10-anthraquinone, alizarin, purpurin) are compared from the point of view of their experimental and computed NMR and UV-visible light absorption spectra. Using an hybrid (explicit/implicit) solvent model, each proton chemical shift can be reproduced with an error less than 7%, even when such protons are engaged in inter-molecular hydrogen bonds with the solvent or when the analyzed sample contains a significant amount of impurities, for instance 9,10-anthraquinone in purpurin. All the steady-state UV-visible absorption spectra feature a significant vibrational progression in the first absorption band. The shape of the corresponding computed spectra, including vibronic couplings obtained with the Adiabatic Hessian approach and the Franck-Condon and Hertzberg-Teller approximation of the transition dipole, are in excellent agreement with the experimental one. The importance and the nature of the vibronic couplings are different for the three molecules, even if they only differ by the number of hydroxyl groups.

1 Introduction

Anthraquinone-based molecules and, especially, the hydroxy-anthraquinone (HAQ) ones (e.g alizarin, purpurin, see Figure 1, but also kermesic and carminic acids, ...) are particularly important in our cultural heritage. Either in their pigment[1–4] or dye forms[5], these chromophores absorb light in different spectral ranges, depending on different parameters such chemical substitutions, *p*H and chemical environment (solvent, metal, inorganic matrix, etc).[6] HAQs can be obtained through extraction of natural plants or insects (eg carminic acid from cochineal[7] or plants (eg alizarin from roots[8]).

Despite the easy access to these molecules and their broad and various light absorption capabilities, HAQ-based paints suffer of a high sensibility to light (UV and/or visible), leading ultimately to a loss of the color, called fading.[4] In a bottom-up perspective, the desire to identify and control the possible fading processes requires a better understanding of HAQ physico-chemical properties. This can be achieved by means of various analytical techniques, among which we herein focus on Nuclear Magnetic Resonance (NMR) spectrometry and UV-visible absorption spectroscopy, as well as those quantum chemical studies aiming at rationalizing the experimental data.

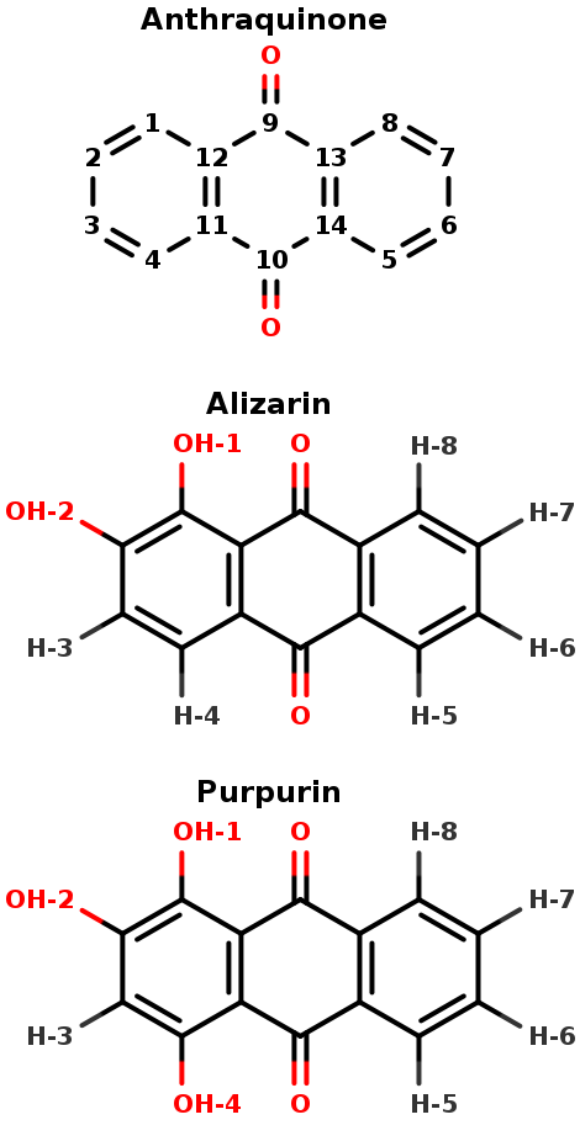

Fig. 1 9,10-anthraquinone, alizarin and purpurin structures, featuring 0, 2 and 3 hydroxyl groups, respectively. The indicated atom labelling is used throughout the present article.

HAQ is any derivative of anthraquinone in which one or several hydrogen atoms are replaced with hydroxyl groups (Figure 1). From the ^{1}H-NMR perspective, 3 main types of protons exist in HAQ, depending on the nuclei to which they are bound: (i) sp^2 carbon participating to an extended conjugated π electronic system, (ii) hydroxy oxygen atoms involved in intra-molecular hydrogen bonds and (iii) hydroxy oxygen atoms involved in inter-molecular hydrogen bonds with the HAQ surroundings. It must be immediately noted that HAQ molecules feature acidic protons and tautomer forms, possibly complicating their chemical spaces,

[a] *Aix-Marseille Univ, CNRS, Institut Chimie Radicalaire, Marseille, France. Fax: +33(0)491288758; Tel: +33(0)413945889; E-mail: nicolas.ferre@univ-amu.fr*
[b] *Sorbonne Université, Laboratoire d'Archéologie Moléculaire et Structurale, Paris, France.*

† Electronic Supplementary Information (ESI) available: 9,10-anthraquinone, alizarin, purpurin tautomers and their free energy differences; natural transition orbital analysis; normal mode analysis; purpurin electrospray mass and ^{1}3-C NMR spectrum.

which in turn complicates the analysis and the interpretation of HAQ ^{1}H-NMR spectra[9,10]. From previous works in which experimental and theoretical NMR spectra of HAQ systems are confronted, it turns out that Density Functional Theory (DFT) is most of the time accurate enough for reaching a 5 to 10% error with respect to the experimental chemical shifts of protons bound to sp^2 carbon atoms.[11–13] Regarding protons involved in intra-molecular hydrogen bonds, a study by Siskos has demonstrated that a 0.1Å variation of the O–H bond length can impact the proton chemical shift by more than 5 ppm[14]. Consequently, the selection of the exchange-correlation functional in DFT, as well as the basis set on which the Kohn-Sham orbitals are expanded, is particularly important. The specific case of protons (partially or totally) shared with the solvent requires a much more involved molecular model: DFT needs to be applied to an extended explicit model featuring the HAQ molecule in interaction with the closest solvent molecules and surrounded by an implicit electrostatic solvent model. Such a complex model is required for reaching an almost quantitative agreement with the experimental spectrum[15]. In ^{1}H-NMR spectroscopy, each and every proton chemical shift is temperature-dependent. It is known for a long time that possible hydrogen-bonding and/or proton exchange with the solvent is witnessed by a much stronger variation of the proton chemical shift with the temperature, a few tenth of ppm each 10K[16–18]. Variable-temperature ^{1}H-NMR is a valuable tool for further characterizing HAQ systems[19]. The expansion (until second order) of the thermal average of the chemical shift constant reveals that the anharmonicity and centrifugation terms are widely responsible of this temperature dependence on the chemical shift in gaz phase.[20] In a solvent, both the chemical shifts and the band full width at half maximum are affected.[21] In HAQ-related systems involving the cathecol function (quercetin, caffeic acid,...) Vassiliki and coworkers have shown that even in organic solvent such as acetone or DMSO, some hydroxyl groups can be involved in a fast proton exchange with the residual water molecules[18]. From the theoretical point of view, such a temperature-based effect has been linked to entropy and can be qualitatively introduced in a extended model built from the solute, the closest solvent molecules to which the solute is hydrogen-bonded and an electrostatic model for the rest of the solvent[22].

UV-visible absorption spectroscopy is a complementary analytical method for investigating the HAQ photophysical properties.[23] These molecules can potentially feature many $n \rightarrow \pi^*$ and $\pi \rightarrow \pi^*$ transitions resulting in spectrum bands whose positions and relative intensities depend on specific intra- and inter-molecular interactions and on the solvent dielectric constant. For instance, the visible region of alizarin in acidic solution presents an absorption maximum about 425 nm attributed to a $\pi \rightarrow \pi^*$ transition[24]. Successive studies confirm the existence of such a broad band around this maximum in various experimental conditions.[25–30]. Refined vibrationnally-resolved UV-visible absorption spectra of several HAQ systems solvated in pentane[23] and more recently for alizarin in n-heptane[31] show a clear vibronic progression, calling for a deeper investigation of its origin. Purpurin vibrationnally-resolved UV-visible absorption spectrum was obtained in water-dioxane mixture at acidic pH. It shows three maxima in the visible region at 455 nm, 480 nm and 510 nm[25]. Purpurin has also been studied in DMSO by Machatová[29]. Three maxima have been identified at 458 nm, 486 nm and 520 nm together with a much less intense absorption band at 600 nm attributed to a proton transfer to the solvent. HAQ UV-visible absorption has also been studied using different theoretical protocols. On one hand, several studies explored the photophysics of alizarin, purpurin and others HAQ molecules using the simplest vertical excitation method at the time-dependent density functional theory (TD-DFT) level.[23,27,32] On the other hand, the UV-visible spectra of alizarin in its protonated form has been obtained within the ensemble framework, taking into account the possible anisotropic solute-solvent interactions.[33] Neither tautomerization nor deprotonation were considered in this study. In order to include vibronic effects, TD-DFT based approaches have been developed[34–36] and successfully applied on molecular systems with similar HAQ skeleton, both in the time-independent[37] and time-dependent[6] frameworks. Jacquemin et al.[37] have highlighted the influence of the basis set (converged spectra are achieved using the 6-311+G* basis set) and the stronger impact of the exchange-correlation functional. Range-separated functionals are necessary to improve the calculated spectra, eventually reaching quantitative agreement with the experimental ones. As already mentioned, HAQ tautomeric forms could exist because of intra-molecular proton transfer between ketone and alcohol moieties. Alizarin tautomers have been studied using several quantum chemical approaches[6,27,32]. In particular, Le person et al.[27] suggest the existence of a tautomeric form by comparing experimental and theoretical absorption spectra. Nevertheless, none of the above mentioned studies succeeded in obtaining a free energy difference between tautomers small enough to account for more than one tautomer at room temperature. More recently, independent theoretical and experimental study suggests that only a single tautomeric form is present in the alizarin ground state.[30,38]

The above-mentioned literature is abundant and manifold. Still, it often lacks a unified picture, in terms of protocols used to analyze and to compare several HAQ compounds. With this idea in mind, we have combined theoretical quantum chemistry calculations with different experimental techniques, namely steady-state UV-visible absorption spectroscopy and NMR spectroscopies, for the investigation and comparison of two molecules representative of the HAQ family: alizarin and purpurin (Figure 1), using 9,10-anthraquinone as a reference.

2 Methodologies

2.1 Calculations

UV-visible spectra have been computed using time-dependent density functional theory (TDDFT) using the ωB97xD exchange-correlation functional[39] and the 6-31+G(d) basis set[40–42]. This level of theory has been extensively tested by different authors in the specific case of vibronic resolved UV-visible spectra of similar compounds.[37] NMR calculations have required another level of theory in order to accurately compute chemical shifts[18]. Therefore the ωB97xD/6-311+G(2d,p) level of theory together with the Gauge-Independent Atomic Orbital approach[43,44] have been used.

The chemical shifts have been obtained by substracting the tetramethyl silane anisotropic shielding tensor to the one of the molecule of interest, both calculated at the same level of theory. The ground state geometry in each system has been optimized using DFT and the same basis sets mentioned above. Potential energy surfaces (PES) of different tautomers and rotamers have been explored. The nature of each stationary point has been confirmed by means of vibrational frequency analysis. The very same workflow has been used in the case of excited state PES using TDDFT. The effect of solvent bulk has been taken into account using the polarizable continuum model (PCM) [45]. Even if some of our experiments have been performed in acetone (alizarin and purpurin) or in heptane (anthraquinone), the recorded NMR spectra have shown specific interactions with solvent molecule and/or water traces. Hence we have also considered the limiting case of water as the bulk. In the case of NMR chemical shift calculations, specific solute-solvent interactions have been taken into account. Therefore, a hybrid cluster+continuum approach using both PCM and explicit solvent molecules close to the solute hydroxyl positions was used. The vibronic resolved UV-Visible spectra have been obtained using the integrated protocols available in Gaussian16, based on the time-dependent approach to vibronic spectroscopy, including both the Franck-Condon (FC) and Herzberg-Teller (HT) terms (the zeroth and first order in the transition dipole moment expansion) in combination with the vertical gradient (VG) or the adiabatic hessian (AH) [36] approaches. A half-maximum (HWHM) equal to 235 cm^{-1} has been used in all spectra. The coupled normal modes have been identified using the time-independent calculation of the very same vibronic couplings [46]. All calculations have been performed using the Gaussian16 code [47], while Natural Transition Orbitals (NTOs) have been produced using the Theodore package [48].

2.2 ^{1}H-NMR experiments

The ^{1}H NMR spectra were carried out on a Bruker Avance III 500 (11.7T) equipped with a wide band broad probe of 5 mm with a frequency of 500.07 MHz. The experiments concerning alizarin and purpurin were performed using either a 90° pulse (zg) sequences and 30° pulse (zg) sequences, respectively. Spectra were recorded using 512 scans for each sample and with a recycling delay of 2s. Temperature-dependent NMR experiments have been performed at 298, 283, 273, 263, 253 or 243K.

2.3 UV-vis experiments

UV-visible experiments have been carried out using Ocean Optics Deuterium-Tungsten Halogen and Ocean Optics Flame detector (FLMS00699) with Ocean Optics QP400-1-UV-VIS glass fibers for acquisition from 200 to 850 nm. Data were collected with OceanView 1.5.0 software in absorption measurement mode, and an average of 100 scans of 4.1 ms integration time was performed for each measurement.

3 Results

3.1 9,10-anthraquinone

9,10-anthraquinone (Figure 1 top, hereafter simply denoted anthraquinone), a highly symmetrical ($\mathscr{D}_{2h}$) molecule in its equilibrium geometry, does not feature any proton which could exchange with the solvent. Accordingly, its spectroscopic properties can be computed straightforwardly. NMR ^{1}H and ^{13}C chemical shifts characterizing the anthraquinone molecule have been reported experimentally by Jiang et al. [49]. We have used DFT calculations to compute these chemical shifts (Table 1). Overall, our results show a good agreement with the reported experimental ones, with an overestimation not larger than 7% . More importantly, the chemical shift differences between non-equivalent nuclei are almost quantitatively reproduced, hence validating the chosen level of theory.

Table 1 Calculated and experimental (measured in DMSO$-d_6$) ^{1}H and ^{13}C chemical shift (δ in ppm) of 9,10-anthraquinone with associated absolute error. Atom labels are available in Figure 1

Atom type and label	Exp.[(a)]	Calc.	Error
^{1}H			
H-1,4,5,8	8.32	8.86	7%
H-2,3,6,7	7.81	8.35	7%
^{13}C			
C-1,4,5,8	127.25	133.55	5%
C-2,3,6,7	134.11	141.31	5%
C-11,12,13,14	133.61	138.57	4%
C-9,10	183.14	192.59	5%

(a) Jiang et al. [49]

The anthraquinone experimental UV-visible absorption spectrum has been previously published by Khan and Khan [23] in n-pentane. Two main bands were reported: the first one in the 275-340 nm region and the second (higher in energy) one in the 210-275 nm region. Herein, we are merely interested in the simulation of the first region which exhibits a small shoulder at 300 nm, as well as 2 clear maxima at 317 nm and 328 nm (Figure 2). Since such fea-

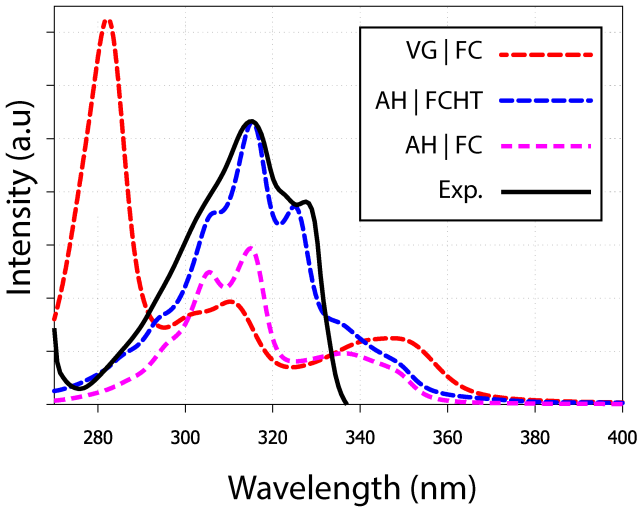

Fig. 2 UV-visible absorption spectra of anthraquinone in n-pentane. Using different methodologies (i) VG|FC; (ii) AH|FCHT and (iii) AH|FC, each calculated spectrum includes at least the six first electronic transitions (see Figure S1). A shift of 55 nm has been applied on all calculated spectra. The experimental spectrum has been extracted from the publication of Khan. [23]

tures could be the signature of vibronic effect, we have decided to test different computational methodologies: (i) Vertical Gradient, (ii) Adiabatic Hessian within the Franck-Condon approximation and (iii) within the Franck-Condon-Herzberg-Teller one, denoted VG|FC, AH|FC and AH|FCHT, respectively. Taking into account the 6 first singlet excited states, the resulting spectra are reported in Figure 2. Overall, only the AH|FCHT-based spectrum satisfactorily fits the experimental one, when a 55 nm red-shift is applied to the computed raw spectrum.

The analysis of the spectrum starts with the vertical transitions in the Franck-Condon region. While the first two lowest transitions are dark $n \rightarrow \pi^*$ ones, the four next ones can be characterized as $\pi \rightarrow \pi^*$ ones (ESI† table T1). In the spectral region of interest, the vertical excitation calculation indicates that two $\pi \rightarrow \pi^*$ electronic transitions, $S_0 \rightarrow S_4$ and $S_0 \rightarrow S_6$, feature a significant oscillator strength, 0.23 and 0.32 respectively, while the two other ones show identically null oscillator strengths. The later result can be easily understood by looking at the symmetry of each hole and particle orbital in a subsequent NTO analysis (Figure 3 and ESI† table S1).

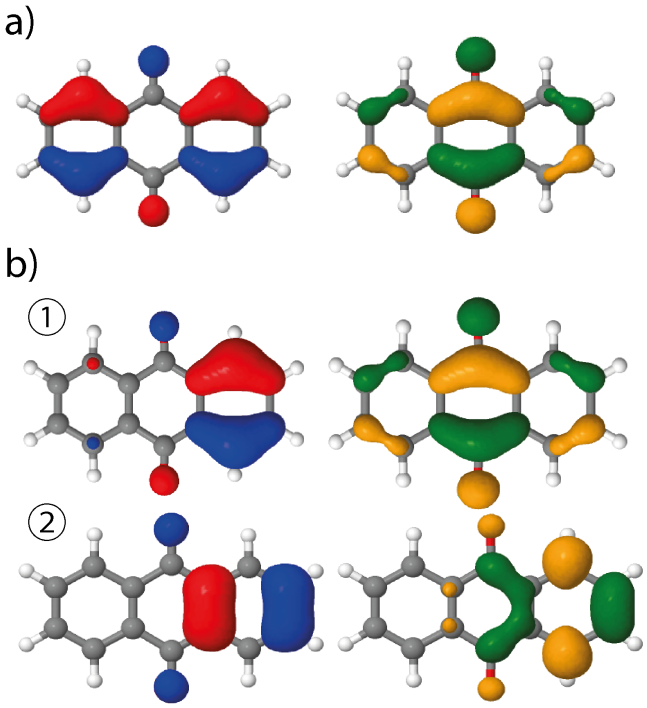

Fig. 3 NTOs of anthraquinone (left: hole orbital; right: particle) involved in the $S_0 \rightarrow S_5$ transitions, using (a) the ground state minimum energy geometry or (b) a modified geometry based on the displacement along the 58th normal mode. This vertical transition features one NTO pair at anthraquinone equilibrium geometry whereas two pairs, ① and ②, are involved at the distorted geometry, the associated coefficients being 0.94 and 0.05, respectively.)

Vibrationnally-resolved spectra obtained from VG|FC or AH|FC vibronic couplings do not compare well with the experimental spectrum. However, using the AH|FCHT approach, the $S_0 \rightarrow S_5$ transition does now contribute significantly to the spectrum (see ESI† figure S1 for a decomposition of the total spectrum into individual contributions). Actually, a single vibronic transition ($|0,0> \rightarrow |5,58>$) corresponding to an in-plane motion (Figure 4), associated to B_{2u} irreducible representation, is responsible for the largest peak. Further evidence of the major role played by this

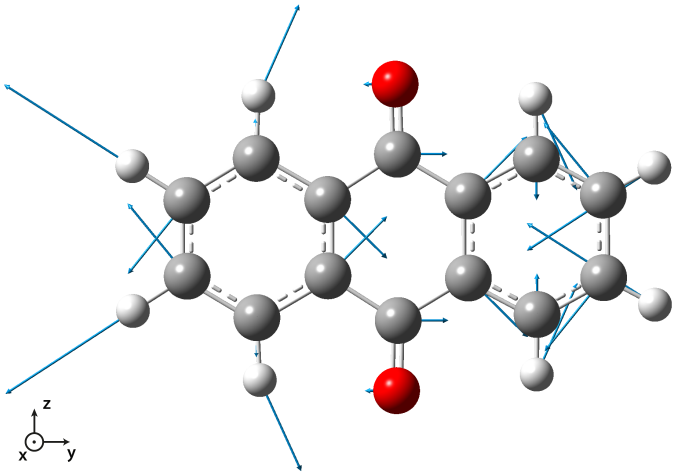

Fig. 4 Vector displacement associated to the normal mode 58 of anthraquinone. All the displayed vectors lie in the molecular plane.

vibration is obtained by manually distorting the anthraquinone geometry along the corresponding normal mode. Using a 5% geometry modification, 2 effects are evidenced: (i) a large increase of the oscillator strength characterizing the $S_0 \rightarrow S_5$ vertical transition ($f = 0.000$ up to $f = 0.062$) and (ii) the localization of the NTO hole in one of the two phenyl moieties (Figure 3). Due to symmetry lowering ($\mathscr{D}_{2h}$ to $\mathscr{C}_{2v}$) of the anthraquinone structure, both the NTOs and their symmetries (in terms of irreducible representation) are affected. While NTOs are delocalized over all the molecule in $\mathscr{D}_{2h}$ symmetry, they localize in some region of the molecule in $\mathscr{C}_{2v}$ symmetry. Note also that the electronic transition $S_0 \rightarrow S_5$ is characterised by a second pair of NTOs in this distorted geometry. Similarly to the $\mathscr{D}_{2h}$ symmetry-based analysis given above, we can explain the finite value of the $S_0 \rightarrow S_5$ oscillator strength using $\mathscr{C}_{2v}$ symmetry elements (ESI† table S1).

In essence, the vibrationnally-induced large modifications of the anthraquinone absorption spectrum can be rationalized by the lowering of the anthraquinone symmetry upon transition to S_5 (with respect to the $\mathscr{D}_{2h}$ geometry in S_0), hence highlighting the importance of including the first order term in the electronic transition dipole moment.

3.2 Alizarin

With respect to anthraquinone, alizarin features two extra and vicinal enol groups (Figure 1 middle). Because of these symmetry-lowering moieties, all the alizarin protons have to be considered as non-equivalent from the NMR point of view (Figure 5 inset). As a matter of fact, the alizarin NMR spectrum recorded in acetone-d_6 features 8 different peaks (Figure 5). Several regions can be distinguished in these spectra: (i) 7 to 8.5 ppm assigned to hydrogen atoms bound to carbon atoms , (ii) 9.5 to 10.5 ppm attributed to the hydroxyl group involved in inter-molecular hydrogen bonds and (iii) 12.75 to 13 ppm corresponding to the hydroxyl group in-

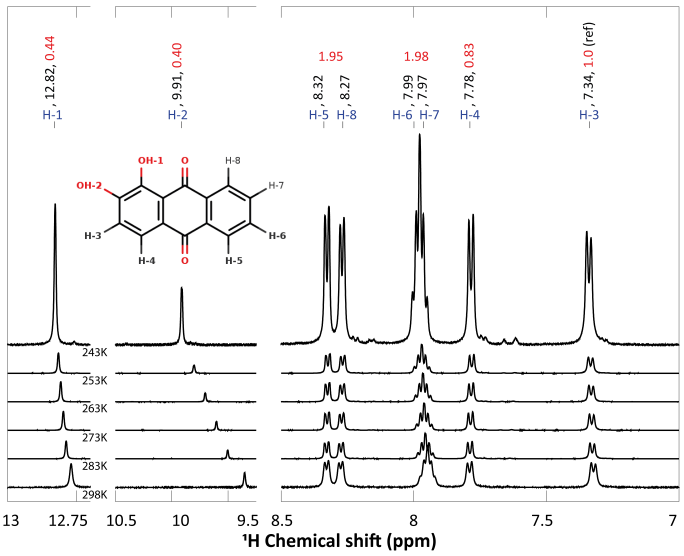

Fig. 5 ^{1}H chemical shift of alizarin in acetone-d_6 (50/50 ratio H_2O/DHO) at different temperatures (243, 253, 263, 273, 283 and 298K). Atom labeling, chemical shifts values (in ppm) and integrated intensities are written in blue, black and red, respectively. The inset represents alizarin and its atom labelling. H-1 is involved in a strong intra-molecular H-bond, whereas H-2 is interacting with the alizarin surrounding.

volved in intra-molecular hydrogen bonds. The attribution of the different protons peaks faces several potential issues that could be solved thanks to quantum chemical computations. First, some of the enol hydrogen atoms can participate into hydrogen bonds, either intermolecular (H-1) or intramolecular (H-2), whose positions can change if alizarin can exist in different tautomer forms resulting from intramolecular proton transfer. Computed free energy differences (ESI† figure S2) strongly suggest that only the most stable tautomer form is present in solution at the temperatures considered in our study, in agreement with a similar finding[32]. When the calculation is repeated in acetone instead of water, the free energies differences do not significantly change. Accordingly, we have considered only the most stable tautomer in the following.

Second, OH proton exchange with the solvent may also be possible, even in acetone-d_6 when some water traces are present. Temperature-dependent NMR spectra are usually helpful in identifying which protons can strongly interact with its surroundings. Accordingly, we have repeated ^{1}H NMR experiments at different temperatures (298, 283, 273, 263, 253 and 243 K, Figure 5) in order to: (i) highlight the bonding mode of each OH proton, ie intra- or inter-molecular; (ii) identify possible chemical exchange events; (iii) allow a better comparison with the computations (performed at 0 K). The most striking result is the strong temperature dependence of the H-2 signal (-0.01 ppm/K). This behavior can simply be explained by the temperature-induced solvent reorganization around H-2, which is the most accessible proton to the solvent.[18]

Turning back to the measured NMR spectrum at 243 K (Figure 5, the integrated peak areas corresponding to OH protons (ie. located between 9 and 14 ppm) are 2 times smaller than the CH ones (region 7-9 ppm). This result can be explained assuming that alizarin co-exists in 2 different forms: (i) the fully protonated form exhibits 8 proton peaks, (ii) the deuterated form resulting from proton exchange with the solvent deuterium can lack one or two protons, ie the enol ones. This explanation has been confirmed by repeating the NMR experiment in non-deuterated acetone.

The experimental and the calculated ^{1}H chemical shifts are summarized in Table 2. Overall, for all alizarin protons, we find chemical shift errors less than 7%, similar to the ones obtained in the case of anthraquinone (Table 1). Note that a cluster approach (in addition of a continuum representation of the solvent) has been employed to improve the computed chemical shift of the proton involved in the inter-molecular hydrogen-bond with the solvent. Therefore, an explicit acetone molecule has been placed close to H-2. Compared to the experimental H-2 chemical shift (9.91 ppm), this procedure demonstrated a noticeable improvement (10.44 ppm) with respect to the unrealistic value (6.08 ppm) obtained without this solvent molecule.

Table 2 Calculated and experimental ^{1}H chemical shifts (in ppm) of alizarin, with errors.

Proton label	Exp.[(a)]	Calc.	Error
H-1	12.82	12.61	2%
H-2	9.91	10.44	5%
H-3	7.34	7.63	3%
H-4	7.78	8.18	3%
H-5	8.32	8.77	5%
H-6	7.99	8.29	6%
H-7	7.97	8.27	3%
H-8	8.27	8.77	6%

(a) Experimental chemical shifts at 243K

The experimental UV-visible absorption spectra of alizarin in polar solvents (acetone, DMSO etc.)[31] do not show any vibrational structure. However, the same authors report a vibrational progression for alizarin in n-heptane (Figure 6 as black full line). Two maxima at 405 and 424 nm are evidenced (not visible in other solvents, see the inset of Figure 6), as well as shoulders at 474, 450 and 388 nm.

Our absorption spectrum computation is performed using an implicit solvent model. Because of convergence issues, we could not use heptane or DMSO as an implicit solvent. Rather, we had to go for a very polar solvent like water in order to ensure correct computational behavior. Therefore the direct comparison between computed and experimental spectra has to be considered as qualitative. According to the TDDFT vertical excitation energies, the first 2 transitions, $S_0 \rightarrow S_1$ and $S_0 \rightarrow S_2$, exhibit similar wavelengths, 363 and 356 nm, respectively. While the first transition has a $\pi \rightarrow \pi^*$ character with an oscillator strength equal to 0.210, the second transition is a forbidden one ($n \rightarrow \pi^*$ with a null oscillator strength), see ESI† figure S4. Transitions to higher excited states are too energetic to contribute to the first absorption band observed experimentally.

The AH|FCHT scheme can be applied when the displacement of the nuclear positions between the ground and excited state is small enough, otherwise the expansion of the electronic dipole moment with respect to normal modes on an exited state will be incorrectly projected, leading to an irrelevant spectrum.[50] Actually, alizarin features an intra-molecular proton transfer (ESIPT)

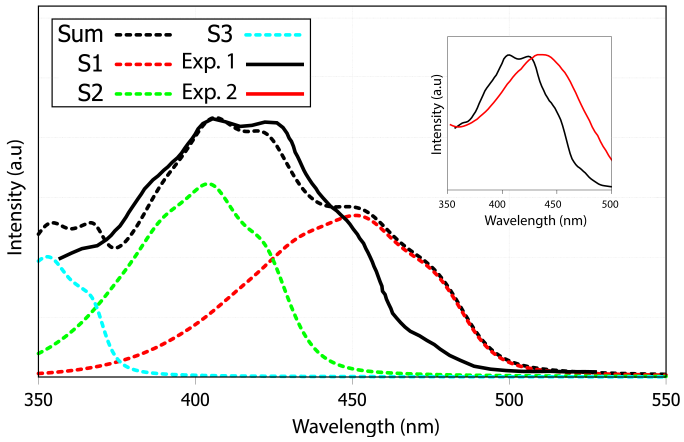

Fig. 6 UV-visible absorption spectrum of alizarin. Experimental results are denoted Exp. 1 and Exp. 2, in heptane (black full line) and DMSO (red full line), respectively. Calculated (black dotted line) absorption spectra of alizarin in water. The calculated spectra is the sum of the first three electronic transitions to S_1, S_2 and S_3 in red, green and blue dashed lines. The calculated spectra have been red-shifted by 55 nm. Two experimental spectra are extracted from Jen et al.[31] and included in the inset. Note the blue-shift and the appearance of the vibrational progression when going from DMSO to heptane.

in the S_1 excited state when a triple-ζ basis set is used[37]. Sticking to a double-ζ basis set avoids any ESIPT and allows us to apply the AH|FCHT approach. The vibronic structure of the first transition, $S_0 \rightarrow S_1$, (Fig. 6, red dashed line) is mainly dominated by in-plane motions involving rocking of C−OH bonds with respect to the aromatic ring. While the $S_0 \rightarrow S_2$ vertical transition is forbidden, applying the AH|FCHT scheme reveals several active vibronic couplings ($|0,0> \rightarrow |2,16>$, $|0,0> \rightarrow |2,21>$, $|0,0> \rightarrow |2,26>$, $|0,0> \rightarrow |2,33>$, $|0,0> \rightarrow |2,35>$ and $|0,0> \rightarrow |2,36>$ associated to $\mathscr{A}$" irreducible representation of $\mathscr{C}_s$ symmetry, represented in ESI† figure S3). These couplings contribute to increase the intensity of this transition, eventually turning to be as intense as the $S_0 \rightarrow S_1$ one (Fig. 6, green dashed line). All the above-mentioned normal modes involve out-of-plane motions, breaking the alizarin $\mathscr{C}_s$ symmetry. The analysis of the alizarin $S_0 \rightarrow S_2$ natural transition orbitals is particularly insightful (Fig. 7). Comparing NTOs for the S_0 optimized geometry and for a displaced one (along the 33th normal mode, ie the one corresponding to the largest vibronic coupling), it is apparent that the n-like hole orbital gains some π character when alizarin motion is taken into account, explaining why the $S_0 \rightarrow S_2$ transition is no longer dark. The consideration of the other coupling modes confirms this analysis.

The final alizarin absorption spectrum is presented in Fig. 6 as black dashed line. The calculated line shape matches well with the reported experimental one[31], highlighting again the importance of using first order terms in the electronic transition dipole moment. Note that the computed-to-experimental 55 nm shift is consistent with the one obtained on similar molecular systems by Jacquemin and coworkers[37]. Improved agreement could have been reached if explicit solvation would have been included into our models. However, vibronic couplings are much more difficult to converge when such specific solute-solvent interactions are considered.

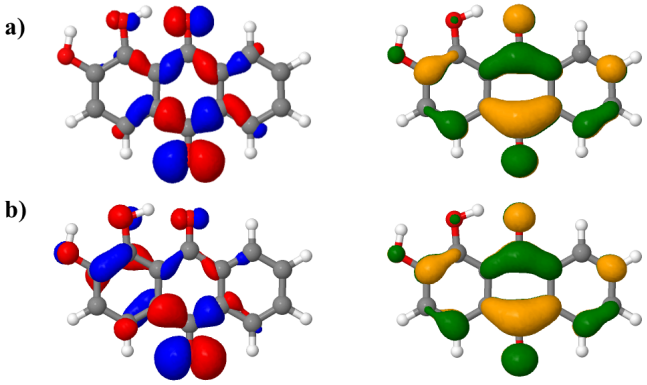

Fig. 7 $S_0 \rightarrow S_2$ natural transition orbitals (NTOs, left: hole, right: particle) of alizarin in a) in its ground state optimized geometry and b) in a displaced geometry using 15% of the displacement corresponding to the 33th normal mode.

3.3 Purpurin

Compared to alizarin, purpurin features an extra enol group, in *para* position with respect to alizarin intramolecular hydrogen-bonded enol group (Figure 1 bottom). Therefore, purpurin can also feature several tautomeric forms as well as several intra- or inter-molecular hydrogen bonds. According to free energy calculations of each tautomer (ESI† figure S5 and Table S4), in gas phase and in condensed phase using a continuum model for the solvent, only one stable form prevails at room temperature, represented in Fig. 8. Experimental NMR ^{1}H spectrum of purpurin in acetone-d_6 is reported in Figure 8. Purpurin, like alizarin and anthraquinone, features different proton families. Firstly, H-1, H-2 and H-4 present a much larger deshielding (chemical shifts comprised between 10.0 and 13.5 ppm) compared to other protons. We can easily attribute them to the three enol moieties. Because only one of them features a temperature-dependent chemical shift, we conclude that there is only one proton (H-2) engaged in an intermolecular hydrogen bond with the solvent. Second, H-5 to H-8 are more deshielded than H-3 and show chemical shifts typical of the benzene molecule (8.5 to 7.75 ppm). Finally, H-3 features a chemical shift (comprised between 6.6 and 6.7 ppm, depending on the temperature) more shielded (compared to benzene), probably due to the enol groups bounded to the same aromatic ring and perturbing the electron density current. These experimental evidences are supported by our quantum chemistry calculations. Considering a cluster composed of the neutral form of purpurin represented in Fig. 8 with an explicit acetone molecule interacting with H-2, we obtain the calculated chemical shifts reported in Table 3. All the 3 families can be clearly identified and their chemical shift differences are correctly reproduced, with an excellent 4% average error. While the low temperature NMR peak attribution is successful, their relative intensities are troublesome. Using H-3 as the reference, the accumulated intensities of the H-5/H-8 or H-6/H-7 pairs appears too large: about 3.5 instead of 2. Increasing the temperature up to 298K, the H-5/H-8 peak is split into two different signals. However, this is not the case for the H-6/H-7 pair.

We have recorded the steady-state UV-visible absorption spectrum of purpurin in acetone-d_6. Its visible contribution (first band)

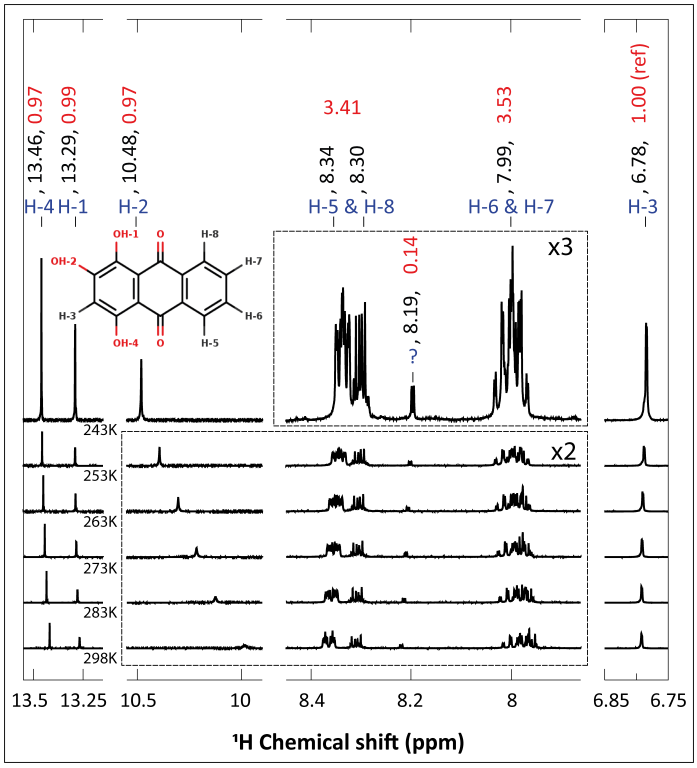

Fig. 8 ^{1}H chemical shift of purpurin in acetone-d_6 at different temperatures (243K, 253, 263, 273, 283 and 298K). Atom labeling, chemical shifts values (in ppm) and integrated intensities are written in blue, black and red, respectively. The inset represents purpurin and its atom labelling. H-1 and H-4 are involved in strong intra-molecular H-bonds, whereas H-2 is interacting with the solvent. The peak marked with '?' at 8.19 ppm is attributed to an impurity. Some parts of the spectra, delimited with dashed lines, have been enlarged with the mentioned zoom ratio.

Table 3 Calculated and experimental ^{1}H chemical shifts (in ppm) of purpurin with individual errors. The corresponding experimental spectrum has been recorded at 243K and is reported in ESI†.

Proton	Exp.	Calc.	Error
H-1	13.29	13.18	1%
H-2	10.48	11.66	10%
H-3	6.78	6.97	3%
H-4	13.46	13.16	2%
H-5	8.34	8.92	7%
H-6	7.99	8.36	4%
H-7	7.99	8.30	4%
H-8	8.3	8.86	6%

is reported in Figure 9 as black full line. This spectrum shows a clear vibrational structure, a maximum intensity at 482 nm and two clear shoulders at 516 and 456 nm. According to our TDDFT calculations, the first 2 raw vertical transitions, $S_0 \rightarrow S_1$ and $S_0 \rightarrow S_2$ are 402 and 339 nm, respectively. While the first transition has a $\pi \rightarrow \pi^*$ character with an oscillator strength equal to 0.27, the second transition is a forbidden one ($n \rightarrow \pi^*$ with a null oscillator strength). The corresponding NTOs are presented in ESI† figure S7. Transitions to higher excited states are too energetic to contribute to the first absorption band observed experimentally.

As already found in the case of alizarin, the AH|FCHT vibronic structure of the $S_0 \rightarrow S_1$ first transition is dominated by in-plane

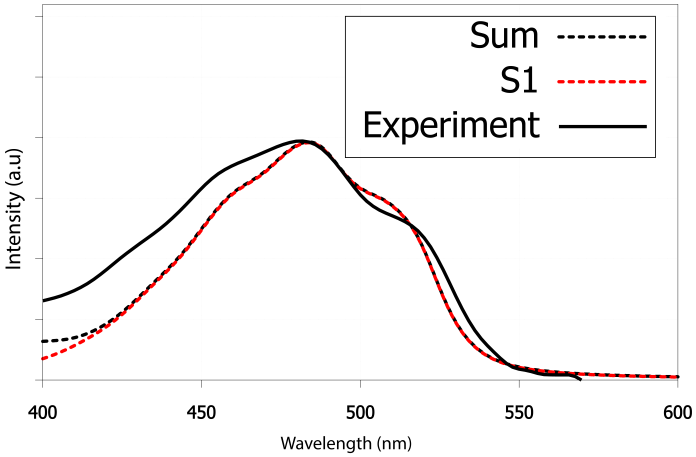

Fig. 9 Experimental and calculated electronic absorption spectra of purpurin in acetone-d_6. Excited states above S_1 only contribute at high excitation wavelengths (shorter than 420 nm).The TDDFT spectrum has been red-shifted by 40 nm to match the experimental maximum wavelength.

motions involving rocking of C−OH bonds with respect to the aromatic ring scissoring (ESI† figure S6). Considering the $S_0 \rightarrow S_2$ transition, the HT term does not bring up sizeable couplings, hence this $n \rightarrow \pi^*$ transition remains forbidden, independently of the solvation model(implicit with different solvents, water or acetone, or with a cluster approach). When red-shifted by 40 nm, the calculated vibrationally resolved absorption spectrum depicted in Fig. 9 as red dashed line is in excellent agreement with the experimental one, confirming that only $S_0 \rightarrow S_1$ contributes to the purpurin first absorption band.

4 Discussions

Three molecules of the anthraquinone family, namely 9,10-anthraquinone, alizarin and purpurin have been studied by means of their respective ^{1}H NMR and UV-visible absorption spectra. As long as a suitable model, including explicit solvent molecules and/or a continuum description of the solvent bulk is included, a good agreement between experiment and computation has been achieved. Since these three molecules only differ by the presence of 0, 2 and 3 hydroxyl moieties, their comparison is of interest.

4.1 UV-visible absorption spectra

While the three UV-vis absorption spectra share the same general shape, it turns out that adding more and more hydroxyl groups is shifting the spectrum from near UV (anthraquinone) to visible (alizarin: violet , purpurin: blue). Moreover, their first absorption band can be characterized by an intense $\pi \rightarrow \pi^*$ vertical transition and several $n \rightarrow \pi^*$ ones, as demonstrated by their respective NTOs (reported in ESI†). However, the calculation of vibronic couplings reveal several important differences we need to discuss further.

In the Franck-Condon approximation[51], two main physical effects can be responsible for a vertical forbidden transition: (i) initial and final vibrational states do not overlap, (ii) the transition dipole moment is null because of symmetry reasons: the direct product of the initial state, final state, position operator irreducible representations does not belong to the fully symmet-

ric one. For instance, anthraquinone $S_0 \rightarrow S_5$ vertical transition is forbidden because of reason (ii). However, the vibronic coupling with a single S_0 normal mode, whose motion lowers the molecule symmetry from $\mathscr{D}_{2h}$ to $\mathscr{C}_{2v}$, is enough to trigger the transition, which eventually becomes the most important one in anthraquinone vibrationnally-resolved first absorption band. At variance with anthraquinone, alizarin first absorption band comprises two vertical transitions, among which one is of $n \rightarrow \pi^*$ character, with a zero oscillator strength. Vibronic couplings are responsible for π/σ mixing in alizarin electronic structure, as evidenced in Figure 7, resulting in a significant increase of its contribution. Eventually, the alizarin first absorption band is made of two contributions with similar weights. While purpurin only contains one more $-$OH group than alizarin, the origin of its visible light absorption is significantly simpler: a single $\pi \rightarrow \pi^*$ contributes. Moreover, its vibronic couplings are solely responsible for the spectrum vibrational progression. As a matter of fact, the extra intramolecular hydrogen bond brought by the third hydroxyl group prevents any structural change which could help π/σ mixing as it was found in the case of alizarin.

To conclude this discussion regarding the modeling of UV-visible light absorption, vibronic couplings are mandatory if ones wants to reproduce 9,10-anthraquinone, alizarin, purpurin, and probably other molecules sharing the same molecular architecture, spectra. Their spectrum vibrational progression is due to triggered forbidden transitions (anthraquinone: increased transition dipole; alizarin: π/σ mixing) and/or regular vibronic couplings of $\pi \rightarrow \pi^*$ transitions (purpurin).

4.2 NMR spectra

Regarding the ^{1}H NMR spectra, we generally obtain a good agreement between the experimental and computed proton chemical shifts when the model takes into account explicit interactions between the solute and the solvent molecules. However, it turns out that the purpurin spectrum (Fig. 8), when compared to anthraquinone and alizarin ones, present unexplained features. Equivalent H-5 and H-8 peaks, as well as equivalent H-6 and H-7 peaks, integrate to a value which is about three times the one obtained for H-3, whereas only two times is expected. This issue is partially solved when increasing the temperature (Fig. 10): the H-5/H-8 signal splits into two peaks which can be integrated separately. At room temperature, we can observe one signal centered at 8.31 ppm and another one at 8.365 ppm with intensities equal to 1 and 2 respectively. Unfortunately, this is not the case for the H-6/H-7 pair. Nevertheless, the comparison of the purpurin chemical shifts (Table 3) with the alizarin spectrum (Figure 5 and Table 2) suggests that signal at 8.365 ppm can be attributed to H-5, the one at 8.31 ppm to H-8 and the one between 7.95 and 8.01 ppm to the pair H-6/H-7. Given their relative intensities (Figure 10), two extra protons need to be introduced: one at 8.365 ppm and one at 7.98 ppm. The identification of the origin of these two protons is not an easy task.

Our first supposition is that the main compound in our sample is not purpurin or corresponds to a degraded form of purpurin which is known to exhibit a weak photoresistance, for instance.[52,53] Repeating the NMR analysis on fresh samples results in identical spectra. Applying electrospray ionization mass spectrometry (in negative mode) to purpurin in acetone, the presence of purpurin was confirmed at at m/z= 255, and supplemented by two additional signals at m/z= 227 and m/z= 183, assigned to purpurin-CO and purpurin-CO$-$CO$_2$ (ESI† figure S8).

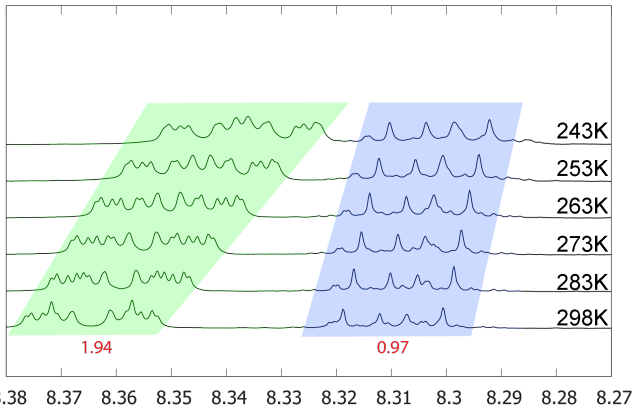

(a) H-5 (green) and H-8 (blue) ^{1}H chemical shifts (ppm)

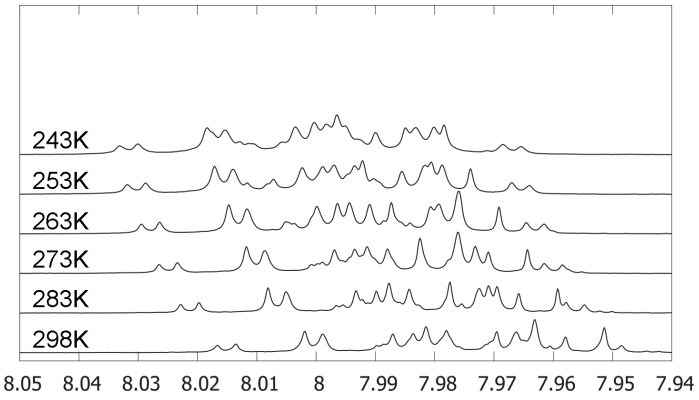

(b) H-6/H-7 ^{1}H chemical shifts (ppm)

Fig. 10 H-5/H-8 (a) and H-6/H-7 (b) ^{1}H chemical shifts for purpurin in acetone-d_6 at various temperatures (243 (top), 253, 263, 273, 283 and 298K(bottom)). Integrated intensities (H-3 being the reference) are written in red. The individual integration of H-5 and H-8 areas can been performed in the spectrum at 298K. However, their signal overlap is too important at 243K to integrate their areas separately.

Hence, we next consider the possibility of the presence of molecules in the sample featuring only two proton chemical shifts at about 8 and 8.35 ppm. The most probable candidate turns out to be 9,10-anthraquinone. As a matter of fact, its proton chemical shifts are 7.81 and 8.32 ppm in DMSO-*d*6 (Table 1). Since the purpurin sample has been solvated in acetone-*d*6 in our experiment, the small differences in the reported chemical shifts can be attributed to the different solvents. Furthermore, the ^{13}C NMR spectrum of purpurin in acetone-d$_6$ exhibits additional signals (for a total of 18) whereas 14 pics are expected (ESI† figure S9). These 4 extra peaks (one at 183.1 ppm, two toward 130 ppm and one at 127 ppm) support our hypothesis of the presence of anthraquinone. Indeed, the chemical shifts are quite in agreement with the ones reported by Jiang et al. in DMSO-d$_6$ (Table 1). Un-

fortunately, 9,10-anthraquinone is not soluble in acetone-*d*6, preventing us to record the corresponding NMR spectrum. Finally, notice that if anthraquinone features two proton NMR signals, each of them corresponds to 4 equivalent protons. Accordingly, the presence of few amounts of anthraquinone in the purpurin sample is expected to significantly contribute to the overall NMR spectrum.

5 Conclusions

In the present work, three anthraquinone-based chromophores have been compared: 9,10-anthraquinone, alizarin and purpurin. While they only differ by the number of hydroxyl substituents (respectively 0, 2 and 3), their corresponding ^{1}H NMR and UV-visible absorption spectra show interesting differences we have investigated.

From the NMR point of view, the comparison of spectra obtained at different temperatures with theoretical spectra computed at 0 K was enough to unambiguously attribute each signal, even in the case of purpurin whose sample presented non negligible traces of anthraquinone. Because of the presence of intermolecular hydrogen bonds between alizarin or purpurin with their solvents, the corresponding theoretical models needs to including a proper description of the solvent effects using both short-range microsolvation and long-range electrostatic couplings with a polarizable continuum.

In the case of the UV-visible absorption spectra, all the three molecules exhibit a first absorption band featuring an important vibrational progression. The latter property has been successfully reproduced with models including vibronic couplings using the Adiabatic Hessian approach and the Franck-Condon+Hertzberg-Teller approximation of the transition dipole moment. Interestingly, these vibronic couplings impact each molecule differently. In anthraquinone, the electronic coupling with symmetry lowering in-plane nuclear motions activate a $\pi \rightarrow \pi^*$ transition, which was found dark when the corresponding vertical transition is considered only. In alizarin, vibronic couplings with out-of-plane nuclear motions induce π/σ mixing which is large enough to trigger the corresponding $n \rightarrow \pi^*$ transition. In purpurin, vibronic couplings are much simpler: they shape the band of the single $\pi \rightarrow \pi^*$ transition.

Finally, even if the three systems studied in this work look apparently chemically similar, we have found that their NMR and UV-visible absorption signatures originate from different microscopic behaviors. This exciting finding prompts us to expand this complementary experimental and computational approach to more involved HAQ systems like carminic acid.

Conflicts of interest

There are no conflicts to declare.

Acknowledgements

Centre de Calcul Intensif d'Aix-Marseille is acknowledged for granting access to its high performance computing resources.

Notes and references

1 D. Guillermin, T. Debroise, P. Trigueiro, L. de Viguerie, B. Rigaud, F. Morlet-Savary, S. Balme, J.-M. Janot, F. Tielens, L. Michot, J. Lalevee, P. Walter and M. Jaber, Dyes and Pigments, 2019, **160**, 971–982.

2 F. Fournier, L. de Viguerie, S. Balme, J.-M. Janot, P. Walter and M. Jaber, Applied Clay Science, 2016, **130**, 12–17.

3 P. Trigueiro, F. A. Pereira, D. Guillermin, B. Rigaud, S. Balme, J.-M. Janot, I. M. dos Santos, M. G. Fonseca, P. Walter and M. Jaber, Dyes and Pigments, 2018, **159**, 384–394.

4 C. Ahn and S. K. Obendorf, Textile Research Journal, 2004, **74**, 949–954.

5 Z. Amar, H. Gottlieb, L. Varshavsky and D. Iluz, BioScience, 2005, **55**, 1080.

6 L. Carta, M. Biczysko, J. Bloino, D. Licari and V. Barone, Physical Chemistry Chemical Physics, 17.

7 M. Borges, R. Tejera, L. Díaz, P. Esparza and E. Ibáñez, Food Chemistry, 2012, **132**, 1855–1860.

8 D. De Santis and M. Moresi, Industrial Crops and Products, 2007, **26**, 151–162.

9 L. Zhu, W. Wang, J. Miao, X. Yin, X. Hu and Y. Yuan, Journal of Molecular Structure, 2017, **1141**, 462–468.

10 L. Kučera, O. Kurka, M. Golec and P. Bednář, Molecules, 2021, **26**, 1–12.

11 D. Flaig, M. Maurer, M. Hanni, K. Braunger, L. Kick, M. Thubauville and C. Ochsenfeld, Journal of Chemical Theory and Computation, 2014, **10**, 572–578.

12 E. Toomsalu and P. Burk, Journal of Molecular Modeling, 2015, **21**, 244.

13 C. Benzi, O. Crescenzi, M. Pavone and V. Barone, Magnetic Resonance in Chemistry, 2004, **42**, S57–S67.

14 M. Siskos, M. Choudhary and I. Gerothanassis, Molecules, 2017, **22**, 415.

15 M. Doskocz, K. Kubas, A. Frąckowiak and R. Gancarz, Polyhedron, 2009, **28**, 2201–2205.

16 J. T. Arnold and M. E. Packard, J. Chem. Phys., 1951, **19**, 1608–1609.

17 N. Muller and R. C. Reiter, The Journal of Chemical Physics, 1965, **42**, 3265–3269.

18 P. Charisiadis, V. Kontogianni, C. Tsiafoulis, A. Tzakos, M. Siskos and I. Gerothanassis, Molecules, 2014, **19**, 13643–13682.

19 C. Shao, Z. She, Z. Guo, H. Peng, X. Cai, S. Zhou, Y. Gu and Y. Lin, Magnetic Resonance in Chemistry, 2007, **45**, 434–438.

20 G. R. Fulmer, A. J. M. Miller, N. H. Sherden, H. E. Gottlieb, A. Nudelman, B. M. Stoltz, J. E. Bercaw and K. I. Goldberg, NMR Chemical Shifts of Trace Impurities: Common Laboratory Solvents, Organics, and Gases in Deuterated Solvents Relevant to the Organometallic Chemist, 2010, vol. 29, pp. 2176—-2179.

21 P. Hore, Nuclear Magnetic Resonance, Oxford University Press, 2015.

22 V. Balevicius and K. Aidas, Applied Magnetic Resonance, 2007, **32**, 363–376.

23 M. S. Khan and Z. H. Khan, Canadian Journal of Analytical Sciences and Spectroscopy, 2002, **47**, 12.

24 A. Navas Diaz, Journal of Photochemistry and Photobiology A: Chemistry, 1990, **53**, 141–167.

25 C. Miliani, A. Romani and G. Favaro, J. Phys. Org. Chem., 2000, **13**, 10.

26 A. Niazi, A. A. Rezaei and F. Shahhosseini, Annali di Chimica, 2007, **97**, 199–211.

27 A. Le Person, J.-P. Cornard and S. Say-Liang-Fat, Chemical Physics Letters, 2011, **517**, 41–45.

28 P. Cysewski, T. Jeliński, M. Przybyłek and A. Shyichuk, New Journal of Chemistry, 2012, **36**, 1836.

29 Z. Machatová, Z. Barbieriková, P. Poliak, V. Jančovičová, V. Lukeš and V. Brezová, Dyes and Pigments, 2016, **132**, 79–93.

30 M. A. P. Turner, M. D. Horbury, V. G. Stavros and N. D. M. Hine, The Journal of Physical Chemistry A, 2019, **123**, 873–880.

31 M. Jen, S. Lee, K. Jeon, S. Hussain and Y. Pang, The Journal of Physical Chemistry B, 2017, **121**, 4129–4136.

32 J. Preat, A. D. Laurent, C. Michaux, E. A. Perpète and D. Jacquemin, Journal of Molecular Structure: THEOCHEM, 2009, **901**, 24–30.

33 T. J. Zuehlsdorff, P. D. Haynes, F. Hanke, M. C. Payne and N. D. M. Hine, Journal of Chemical Theory and Computation, 2016, **12**, 1853–1861.

34 F. Santoro, R. Improta, A. Lami, J. Bloino and V. Barone, The Journal of Chemical Physics, 2007, **126**, 084509.

35 F. Santoro, A. Lami, R. Improta, J. Bloino and V. Barone, The Journal of Chemical Physics, 2008, **128**, 224311.

36 A. Baiardi, J. Bloino and V. Barone, Journal of Chemical Theory and Computation, 2013, **9**, 4097–4115.

37 D. Jacquemin, E. Brémond, A. Planchat, I. Ciofini and C. Adamo, Journal of Chemical Theory and Computation, 2011, **7**, 1882–1892.

38 A. Amat, C. Miliani, A. Romani and S. Fantacci, Phys. Chem. Chem. Phys., 2015, **17**, 6374–6382.

39 J.-D. Chai and M. Head-Gordon, The Journal of Chemical Physics, 2009, **131**, 174105.

40 R. Ditchfield, W. J. Hehre and J. A. Pople, The Journal of Chemical Physics, 1971, **54**, 724–728.

41 W. J. Hehre, R. Ditchfield and J. A. Pople, The Journal of Chemical Physics, 1972, **56**, 2257–2261.

42 P. C. Hariharan and J. A. Pople, Theoretica Chimica Acta, 1973, **28**, 213–222.

43 J. Gauss, Berichte der Bunsengesellschaft für physikalische Chemie, 1995, **99**, 1001–1008.

44 J. R. Cheeseman, G. W. Trucks, T. A. Keith and M. J. Frisch, The Journal of Chemical Physics, 1996, **104**, 5497–5509.

45 J. Tomasi, B. Mennucci and R. Cammi, Chemical Reviews, 2005, **105**, 2999–3094.

46 M. Biczysko, J. Bloino, F. Santoro and V. Barone, in Time-Independent Approaches to Simulate Electronic Spectra Lineshapes: From Small Molecules to Macrosystems, John Wiley & Sons, Ltd, 2011, ch. 8, pp. 361–443.

47 M. J. Frisch, G. W. Trucks, H. B. Schlegel, G. E. Scuseria, M. A. Robb, J. R. Cheeseman, G. Scalmani, V. Barone, G. A. Petersson, H. Nakatsuji, X. Li, M. Caricato, A. V. Marenich, J. Bloino, B. G. Janesko, R. Gomperts, B. Mennucci, H. P. Hratchian, J. V. Ortiz, A. F. Izmaylov, J. L. Sonnenberg, D. Williams-Young, F. Ding, F. Lipparini, F. Egidi, J. Goings, B. Peng, A. Petrone, T. Henderson, D. Ranasinghe, V. G. Zakrzewski, J. Gao, N. Rega, G. Zheng, W. Liang, M. Hada, M. Ehara, K. Toyota, R. Fukuda, J. Hasegawa, M. Ishida, T. Nakajima, Y. Honda, O. Kitao, H. Nakai, T. Vreven, K. Throssell, J. A. Montgomery, Jr., J. E. Peralta, F. Ogliaro, M. J. Bearpark, J. J. Heyd, E. N. Brothers, K. N. Kudin, V. N. Staroverov, T. A. Keith, R. Kobayashi, J. Normand, K. Raghavachari, A. P. Rendell, J. C. Burant, S. S. Iyengar, J. Tomasi, M. Cossi, J. M. Millam, M. Klene, C. Adamo, R. Cammi, J. W. Ochterski, R. L. Martin, K. Morokuma, O. Farkas, J. B. Foresman and D. J. Fox, Gaussian~16 Revision C.01, 2016, Gaussian Inc. Wallingford CT.

48 F. Plasser, The Journal of Chemical Physics, 2020, **152**, 084108.

49 H. Jiang, H. Sun, S. Zhang, R. Hua, Y. Xu, S. Jin, H. Gong and L. Li, Journal of Inclusion Phenomena and Macrocyclic Chemistry, 2007, **58**, 133–138.

50 J. Bloino, A. Baiardi and M. Biczysko, International Journal of Quantum Chemistry, 2016, **116**, 1543–1574.

51 P. W. Atkins and R. S. Friedman, Molecular Quantum Mechanics, Oxford University Press, Oxford, New York, Fifth Edition edn, 2010.

52 S. Ahmadi, G. Absalan, D. Craig and D. Goltz, Dyes and Pigments, 2014, **105**, 57–62.

53 C. Clementi, W. Nowik, A. Romani, F. Cibin and G. Favaro, Analytica Chimica Acta, 2007, **596**, 46–54.